SCIENCE CHINA Materials ARTICLES

mater.scichina.com link.springer.com

Published online 8 April 2020 | https://doi.org/10.1007/s40843-020-1292-6
*Sci China Mater* 2020, 63(7): 1205–1215

# Oxygen vacancies-rich cobalt-doped $NiMoO_4$ nanosheets for high energy density and stable aqueous Ni-Zn battery

Yuenian Shen[1], Ke Zhang[4], Fang Yang[4], Zhihao Li[1], Zhe Cui[1], Rujia Zou[1], Qian Liu[3*], Junqing Hu[5] and Kaibing Xu[1,2*]

**ABSTRACT** **The enhancement of energy density and cycling stability is in urgent need for the widespread applications of aqueous rechargeable Ni-Zn batteries. Herein, a facile strategy has been employed to construct hierarchical Co-doped $NiMoO_4$ nanosheets as the cathode for high-performance Ni-Zn battery. Benefiting from the merits of substantially improved electrical conductivity and increased concentration of oxygen vacancies, the $NiMoO_4$ with 15% cobalt doping (denoted as CNMO-15) displays the best capacity of 361.4 mA h $g^{-1}$ at a current density of 3 A $g^{-1}$ and excellent cycle stability. Moreover, the assembled CNMO-15//Zn battery delivers a satisfactory specific capacity of 270.9 mA h $g^{-1}$ at 2 A $g^{-1}$ and a remarkable energy density of 474.1 W h $kg^{-1}$ at 3.5 kW $kg^{-1}$, together with a maximum power density of 10.3 kW $kg^{-1}$ achieved at 118.8 W h $kg^{-1}$. Noticeably, there is no capacity decay with a 119.8% retention observed after 5000 cycles, demonstrating its outstanding long lifespan. This work might provide valuable inspirations for the fabrication of high-performance Ni-Zn batteries with superior energy density and impressive stability.**

**Keywords:** $NiMoO_4$ nanosheets, oxygen vacancies, Ni-Zn batteries, energy density, cycle stability

## INTRODUCTION

Facing up with energy crisis and worsening environment, the popularization and utilization of clean energy are of significant importance. Limited by the conversion and transmission of these energies, highly-efficient and portable electrochemical storage devices have undergone tremendous development in recent years [1–3]. As the most widely used energy storage devices commercially, lithium-ion batteries possess the advantages of high capacity, superior energy density and stable charging-discharging performance. However, the safety issues mainly caused by the unavoidable formation of lithium dendrite, as well as insufficient power density and high cost, severely hinder their further applications [4-7]. Alternatively, conventional aqueous alkaline rechargeable batteries with the merits of high safety, outstanding power density and abundant resources, have received much more attention recently, such as Ni-Fe [8,9], Ni-Co [10,11], Ni-Bi [7,12], and Ni-Zn batteries [13,14]. Particularly, the Ni-Zn batteries hold great promise in energy storage area because of their high output voltage (~1.8 V) compared with that of other aqueous batteries (most ≤ 1.2 V), abundant reserve of Zn, and low toxicity [15,16]. Unfortunately, the poor energy density and cycling stability of Ni-Zn batteries are still important bottlenecks in the practical energy storage applications [14,17]. An efficient way to settle the poor energy density is combing Ni-Zn batteries with Zn-air batteries. Integrating these two kinds of batteries into a single one by sharing the same anode, both high discharge voltage (originating from Ni-Zn battery) and high capacity (benefiting from Zn-air battery) can be accomplished in the Zn-Ni/air hybrid batteries simultaneously [18–20]. In this way, the weak energy density gets well addressed but the cycling

[1] State Key Laboratory for Modification of Chemical Fibers and Polymer Materials, College of Materials Science and Engineering, Donghua University, Shanghai 201620, China
[2] Research Center for Analysis and Measurement, Donghua University, Shanghai 201620, China
[3] Department of Applied Physics, Donghua University, Shanghai 201620, China
[4] College of Mechanical and Automotive Engineering, Shanghai University of Engineering Science, Shanghai 201620, China
[5] College of Health Science and Environmental Engineering, Shenzhen Technology University, Shenzhen 518118, China
* Corresponding authors (emails: qianliu@dhu.edu.cn (Liu Q); xukaibing@dhu.edu.cn (Xu K))

  

stability still remains an unsolved problem. As is known to all, the performance of Ni-Zn batteries is dominantly determined by the intrinsic properties of electrode materials. Compared with the high theoretical capacity of Zn anode (820 mA h $g^{-1}$), the capacities of most Ni-based cathode materials reported previously are relatively low, impeding the enhancement of energy density for Ni-Zn batteries [21–23]. Therefore, varieties of Ni-based materials have been intensively explored and shown improved capacities for Ni-Zn batteries, such as NiO [22], $Ni(OH)_2$ [24], and Ni@NiO [17]. For example, Gong *et al.* [25] assembled a high-performance Ni-Zn battery with NiAl-Co-layered double hydroxide attached to carbon nanotubes as the cathode, delivering a remarkable specific capacity of 184 mA h $g^{-1}$ (at 3.5 A $g^{-1}$) and an impressive energy density of 324 W h $kg^{-1}$ (at ~4.0 kW $kg^{-1}$). Despite these achievements, the fabrication of Ni-based cathodes with larger specific capacities is still highly urgently needed.

Benefiting from the multiple oxidation states and competitive electrical conductivity, ternary metal oxides, such as $NiMoO_4$ [26,27], $CoMoO_4$ [28,29] and $NiCo_2O_4$ [30,31], have attracted considerable interests in various energy storage devices. In particular, $NiMoO_4$ outperforms among these ternary metal oxides by the great reaction activity of nickel and superior electron transfer rate of molybdenum [26,32]. For instance, Sharma *et al.* [33] reported the synthesis of ultrasmall $NiMoO_4$ nanoclusters on active carbon, displaying a high specific capacity of 184.7 mA h $g^{-1}$ at a current density of 1 A $g^{-1}$. Disappointingly, the obtained capacities of $NiMoO_4$ electrodes are still far from expectation because of its inferior electrical conductivity and limited electroactive sites [27,29,31]. The metal doping is considered to be a promising approach to boost the capacity performance of electrode materials. During the doping process, the concentration of oxygen vacancies can get strengthened, which serve as shallow donors to adjust the band gap and tune the electron structure, consequently improving the electrical conductivity [22,24,25,34]. Simultaneously, oxygen vacancies can also act as extra active sites for redox reactions to enhance the electrochemical properties [35–37]. Therefore, it is urgently desirable to develop metal doping $NiMoO_4$ electrodes for reinforcing energy density and cycle life of aqueous rechargeable Ni-Zn batteries.

Herein, we have successfully tackled the limited energy density and poor cycling performance of $NiMoO_4$ electrode with the strategy of cobalt doping, which were prepared by a facile hydrothermal process followed by calcination treatment. Attributed to the abundant oxygen vacancies generated from the doping process, the band gap and electron structure get optimized, consequently boosting the intrinsic electrical conductivity of $NiMoO_4$. Meanwhile, these oxygen vacancies can also participate in the redox reactions as extra active sites, which is beneficial for achieving a superior energy density. As a result, the $NiMoO_4$ with 15% cobalt doping (CNMO-15) displays the best capacity of 361.4 mA h $g^{-1}$ at a current density of 3 A $g^{-1}$ compared with pure $NiMoO_4$ (206.4 mA h $g^{-1}$ at 3 A $g^{-1}$), and better cycle stability (remaining 95.7% of initial capacity after 3000 cycles). Furthermore, an aqueous alkaline Ni-Zn battery was assembled with CNMO-15 as the cathode and a commercial Zn plate as the anode. The obtained device delivers a favorable energy density of 474.1 W h $kg^{-1}$ at a power density of 3.5 kW $kg^{-1}$. Most importantly, there is no decay with a 119.8% retention observed after 5000 cycles.

## EXPERIMENTAL SECTION

### Preparation of Co-doped $NiMoO_4$ nanosheet arrays on Ni foam

All reagents were of analytical grade (purchased from Sinopharm) and used directly without any further purification. The Co-doped $NiMoO_4$ nanosheet arrays were synthesized by a hydrothermal treatment, followed by a calcination process. Taking the preparation of CNMO-15 as an example, 0.85 mmol of $NiCl_2{\cdot}6H_2O$ with 0.15 mmol of $CoCl_2{\cdot}6H_2O$, and 1 mmol of $NaMoO_4{\cdot}2H_2O$ were dissolved in 50 mL of deionized water homogeneously, and then transferred into a 60-mL Teflon lined stainless-steel autoclave. A piece of Ni foam (1 × 4 $cm^2$) with pretreatment was immersed into the solution and stood against the wall. After that, the autoclave was sealed and maintained at 120°C for 5 h. The obtained Ni foam with active materials was washed by deionized water and ethanol alternatively and then dried at 60°C for 24 h. Finally, the Ni foam was calcined in nitrogen at 350°C for 2 h and cooled to room temperature naturally.

For comparison, the Co-doped $NiMoO_4$ nanosheet arrays on Ni foam with different doping levels of cobalt (0%, 5%, 10% and 20%) were fabricated by precisely regulating the molar ratio of Ni/Co salts in the precursor solution with the same total amount of metal ions (1 mmol), denoted as NMO, CNMO-5, CNMO-10 and CNMO-20, respectively. The mass loading of Co-doped $NiMoO_4$ nanosheets was about 0.8 mg $cm^{-2}$ on average.

### Materials characterization

The morphology and micro-/nanostructures of the as-obtained materials were investigated using a scanning

  

electron microscopy (SEM; Hitachi, S-4800) and a transmission electron microscopy (TEM; JEOL, JEM-2100F) with energy-dispersive X-ray spectrometry (EDS). The phase compositions and elemental valance states were analyzed by X-ray diffraction (XRD; Rigaku, D/max-2550 PC) employing Cu-Kα as radiation and X-ray photoelectron spectroscopy (XPS; Thermo Fisher, Escalab 250Xi) calibrated by referencing the C 1s to 284.8 eV.

### Electrochemical measurements

The electrochemical performance of electrode materials was measured through a three-electrode mode on an electrochemical workstation (PGSTAT302N potentiostat, Metrohm Autolab, Utrecht, the Netherlands). The obtained Ni foam loaded with active materials was used directly as working electrode, when a saturated calomel electrode (SCE) and platinum (Pt) acted as reference electrode and counter electrode, respectively.

For the assembly of aqueous alkaline battery, the obtained CNMO-15 electrode ($1 \times 1\ cm^2$) was used as cathode while a piece of commercial Zn plate with same area was used as the anode. And a separator (NKK separator, Nippon Kodoshi Corporation, Kochi, Japan) was sandwiched in the middle of cathode and anode. The electrolyte was prepared by a mixture solution comprising of 1 mol $L^{-1}$ KOH and 0.01 mol $L^{-1}$ $Zn(CH_3COO)_2$. The whole device was encapsulated in a small plastic bag with part of electrodes kept outside. The electrochemical performance of Ni-Zn battery was also detected on the same electrochemical workstation.

The specific capacity (mA h $g^{-1}$) was calculated according to the equation: $C = I \times \Delta t/m$, where $I$ (mA) is the discharge current, $\Delta t$ (h) is the discharge time, and $m$ (g) is the mass of active material. The energy density (W h $kg^{-1}$) and power density (W $kg^{-1}$) were figured based on the formulas: $E = C \times V$ and $P = E/t$, where $C$ (mA h $g^{-1}$), $V$ (V) and $t$ (h) represent the specific capacity, discharging plateau and time of CNMO-15//Zn battery, respectively.

## RESULTS AND DISCUSSION

As described schematically in Fig. 1a, the vacancy-rich Co-doped $NiMoO_4$ nanosheets were obtained by a facile and accessible two-step synthetic routine. Firstly, the precursor of Co-doped $NiMoO_4$ nanosheets on Ni foam was synthesized by a simple hydrothermal procedure by controlling the doping mass of cobalt. And then, the acquired precursor was annealed under nitrogen atmosphere, transforming into Co-doped $NiMoO_4$ nanosheets. The as-obtained Co-doped $NiMoO_4$ nanosheets are a promising electrode material for electrochemical energy storage, mainly attributed to its hierarchical nanostructure and chemical composition, as schematically illustrated in Fig. 1b. On the one hand, the interconnected vertically Co-doped $NiMoO_4$ nanosheets provide dense electroactive sites for redox reaction, and the open space between these nanosheets can act as a robust reservoir for electrolyte ion penetration to improve the diffusion kinetics. On the other hand, the Co doping can boost the intrinsic electrical conductivity of $NiMoO_4$ and create active defects, resulting in optimized utilization of electrode materials. Among the Co-doped $NiMoO_4$ nanosheets with different doping levels of cobalt, CNMO-15 displays the best electrochemical performance. As a result, an aqueous alkaline Ni-Zn battery was assembled by CNMO-15 as the cathode and a commercial Zn plate as the anode (Fig. 1c), with the mixed solution of 1 mol $L^{-1}$ KOH and 0.01 mol $L^{-1}$ $Zn(CH_3COO)_2$ as electrolyte, denoted as CNMO-15//Zn.

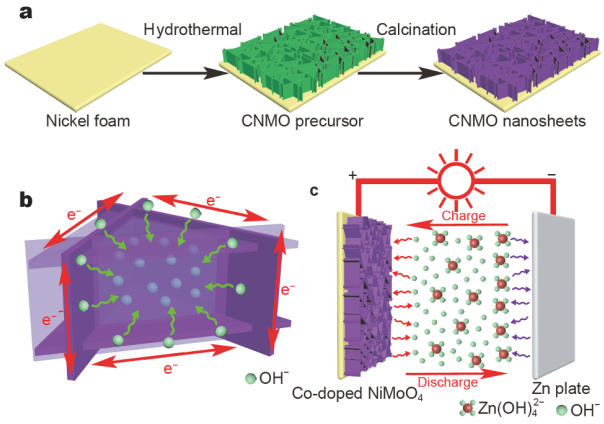


**Figure 1** Illustration of (a) the synthetic process for Co-doped $NiMoO_4$ nanosheets, (b) electron transport in the porous nanostructure and (c) assembled structure of CNMO-15//Zn battery.

The morphology and microstructure of the CNMO-15 nanosheets were characterized by SEM and TEM. As could be seen clearly from Fig. 2a and b, numerous interconnected nanosheets grew vertically and densely on the Ni foam substrate. Such nanosheets forming hierarchical nanostructure with high specific surface area provided abundant active sites for fast redox reaction. Meanwhile, charges could transfer rapidly along the skeleton of nanosheets. Particularly, lots of enclosed spaces were constructed by the ordered stacked hierarchical nanosheets, which served as micro-reservoirs of electrolyte. Moreover, compared with the pure $NiMoO_4$

  

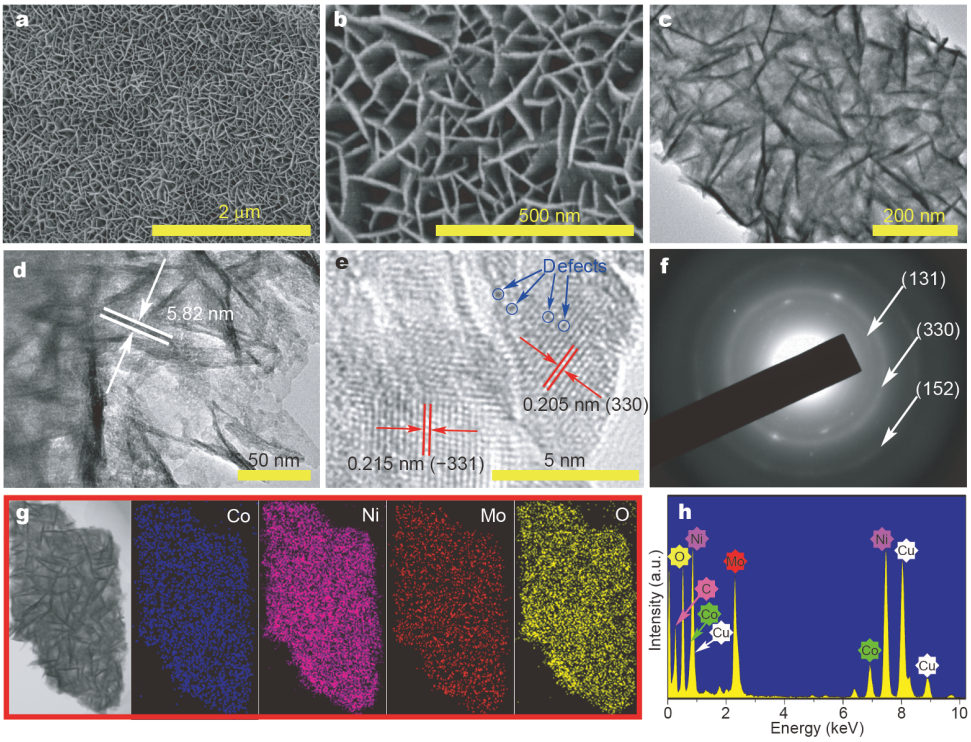


**Figure 2** (a, b) SEM images, (c, d) TEM images, (e) high resolution TEM image, (f) SAED, (g) elemental mapping images and (h) EDS analysis of CNMO-15 nanosheets.

nanosheets (Fig. S1), there was no obvious structural change, indicating the structural stability of $NiMoO_4$ nanosheets. The hierarchical nanosheet-assembled nanostructure of CNMO-15 could be further illustrated by TEM images (Fig. 2c and d). The interlaced nanosheets had an average thickness of 5.82 nm. Importantly, plentiful pores could also be found on the nanosheets, furnishing high-speed channels for ion diffusion. Seen from the clearly resolved lattice fringes shown in Fig. 2e, the interplanar distances of 0.205 and 0.215 nm well-corresponded to (330) and (-331) planes of $NiMoO_4$. For the pristine $NiMoO_4$ nanosheets, the interplanar distance of 0.246 nm (Fig. S2) corresponded well to (131) plane of $NiMoO_4$ (JCPDS No. 86-0361), consistent with the selected area electron diffraction (SAED) patterns (Fig. S3). Besides, we could conclude the existence and even distribution of Ni, Mo, O elements in the nanosheets based on Figs S4 and S5. Simultaneously, structural defects could be observed for the CNMO-15 nanosheets as the blue arrows pointed, generating from the cobalt doping. Moreover, diffraction rings in the SAED patterns (Fig. 2f) could be indexed to (131), (330) and (152) planes of $NiMoO_4$ (JCPDS No. 86-0361). Furthermore, the elemental mapping images in Fig. 2g verified that Co, Ni, Mo and O elements distributed uniformly throughout the entire nanosheets. The existence of Co, Ni, Mo and O elements could also be demonstrated by the EDS analysis (Fig. 2h). Additionally, the morphologies of CNMO-5, CNMO-10 and CNMO-20 under different magnifications were shown in Fig. S6 as well, which could be inferred that the nanosheet structure remained almost unchanged with the increase in mass of cobalt doping.

XRD and XPS were applied to analyze the phase compositions and elemental states. However, the XRD patterns (Fig. S7) could not be utilized as evidence to prove the existence of $NiMoO_4$ phase since no related peaks were observed. Due to the low mass loading of active materials on Ni foam, only three apparent peaks ($2\theta$ = 44.4°, 51.8° and 76.3°) corresponding to Ni (JCPDS No. 70-1849) could be detected. Importantly, the survey spectrum of CNMO-15 (Fig. S8) indicated the co-existence of Co, Ni, Mo and O elements. Furthermore, XPS spectrum of Co 2p (Fig. 3a) revealed binding energies of Co $2p_{3/2}$ and Co $2p_{1/2}$ centered at 780.8 and 796.7 eV with a binding-energy gap of 15.9 eV, as well as two satellite peaks at 785.3 and 803.1 eV. These characteristic peaks were assigned to $Co^{2+}$, certifying the valid doping of cobalt atoms [29,38-40]. In Fig. 3b, Ni $2p_{3/2}$ (855.6 eV) and

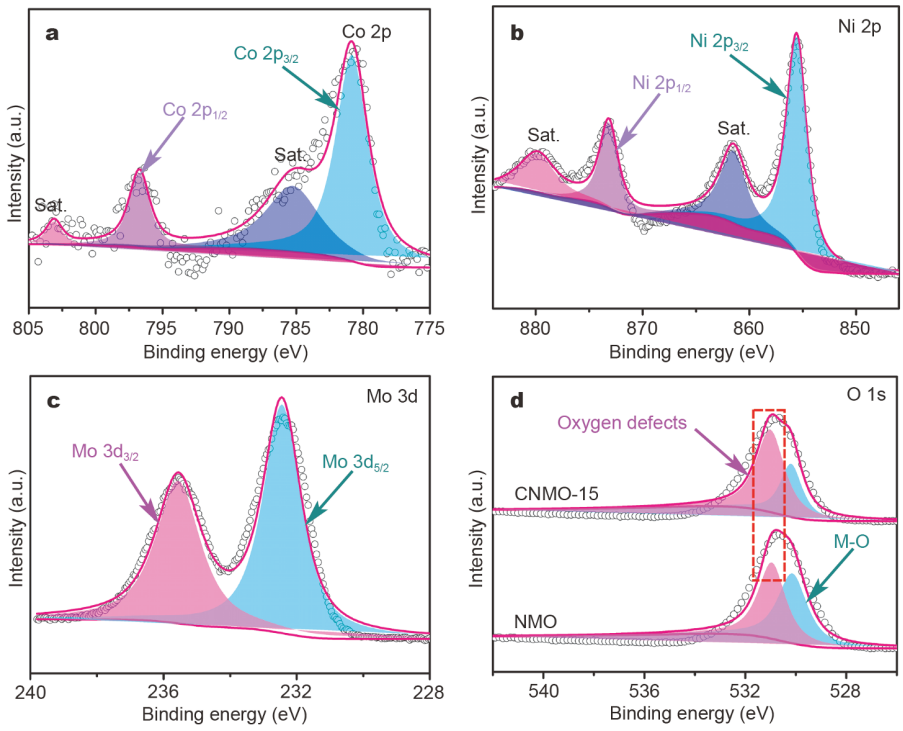


**Figure 3** High-resolution XPS spectra of (a) Co 2p, (b) Ni 2p, (c) Mo 3d and (d) O 1s for CNMO-15 nanosheets.

Ni $2p_{1/2}$ (873.2 eV) with a binding-energy gap of 17.6 eV, accompanied by two shakeup satellites at a binding energy of 861.5 and 879.8 eV, respectively, indicated the presence of $Ni^{2+}$ [26,27,39]. Meanwhile, two peaks located at 232.5 eV (Mo $3d_{5/2}$) and 235.6 eV (Mo $3d_{3/2}$) with a binding-energy gap of 3.1 eV, representing the characteristic peaks of $Mo^{6+}$ (Fig. 3c) [26,33,41]. More importantly, the O 1s spectrum of CNMO-15 (Fig. 3d) could be deconvoluted into two components, two peaks centering at 530.1 and 531.0 eV indexed to the M–O bond and oxygen defects, respectively [21,27]. Noticeably, the peak of CNMO-15 belonging to oxygen defects got strengthened compared with NMO, illustrating the introduction of cobalt effectively improved the concentration of oxygen defects. This improvement was beneficial for the enhancement of electron transfer and consequently enlarged electrical conductivity, finally boosting the activity of redox reactions. Combining XPS analysis with other characterization methods mentioned above, we could infer that Co-doped $NiMoO_4$ nanosheets have been synthesized successfully.

The electrochemical performance of Co-doped $NiMoO_4$ was performed on a three-electrode device in 1 mol $L^{-1}$ KOH solution. Fig. 4a displays the comparative cyclic voltammetry (CV) curves of NMO and CNMO-15 electrodes at a scan rate of 10 mV $s^{-1}$. The enclosed area and the corresponding current density of CNMO-15 were much larger than that of NMO electrode, demonstrating enhanced capacity, which was caused by the boost of electrical conductivity and reaction activity due to the cobalt doping. Additionally, the CV integrated area of the pure Ni foam was negligible as compared with that of the CNMO-15 electrode (Fig. S9), revealing that almost no capacity contribution comes from the Ni foam. We could get the same conclusion according to galvanostatic charge-discharge (CD) curves (Fig. 4c), where the discharging time of CNMO-15 was much longer than that of other electrodes at the same current density of 3 A $g^{-1}$. As depicted by the CV curves of CNMO-15 electrode in Fig. 4b, the good symmetry and similar shapes represent highly reversibility and stability of the redox reaction occurred on the electrode when the scan rates increased from 10 to 50 mV $s^{-1}$. Meanwhile, the CNMO-15 electrode delivered an advanced specific capacity of 361.4 mA h $g^{-1}$ at a current density of 3 A $g^{-1}$, and still kept 200.6 mA h $g^{-1}$ even at a high current density of 20 A $g^{-1}$ (Fig. 4d). These outstanding electrochemical properties exceeded most of other electrodes, for instance, NiO-carbon nanotube composite (155.0 mA h $g^{-1}$ at 1 A $g^{-1}$) [22], $Co_3O_4$@NiO nanostrip@nanorod arrays (242.4 mA h $g^{-1}$ at 5 mA $cm^{-2}$)

  

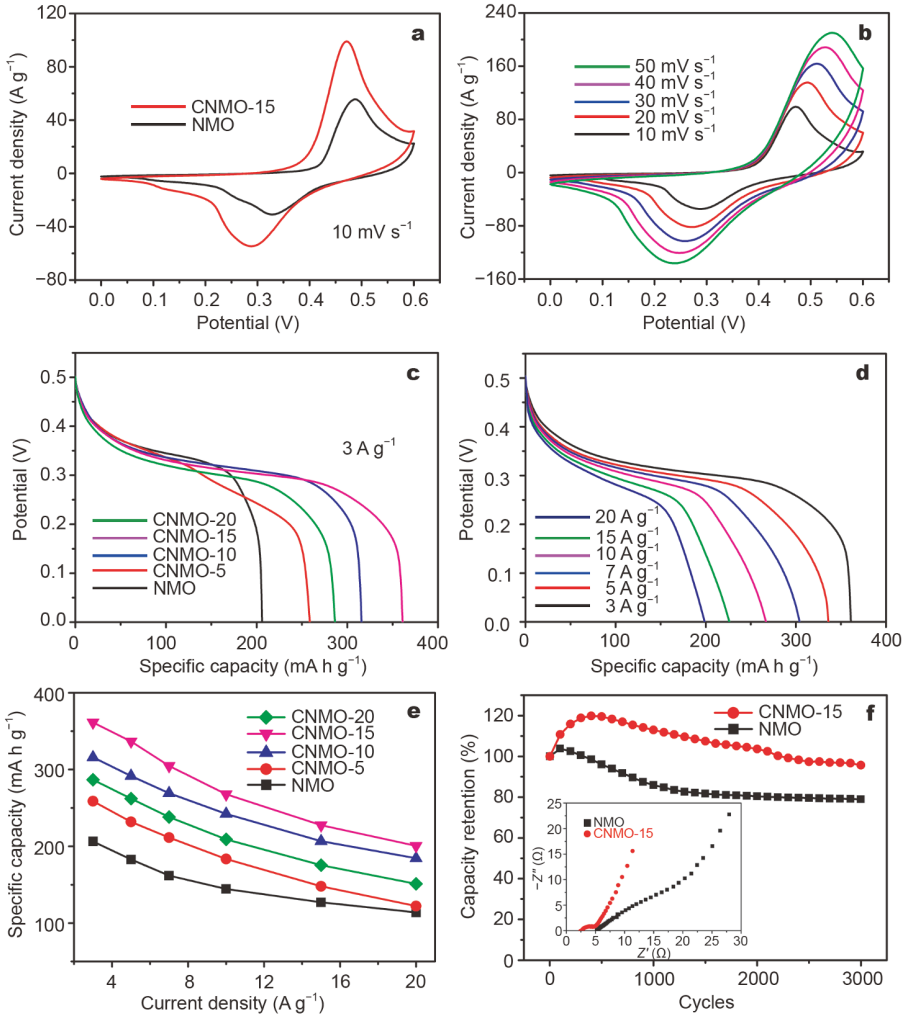


**Figure 4** (a) CV curves, (c) CD curves, (e) specific capacity and (f) cycling tests at 60 mV $s^{-1}$ and Nyquist plots (inset) of the Co-doped $NiMoO_4$ electrodes. (b) CV curves and (d) CD curves of the CNMO-15 electrode.

[42], $NiS_2$/reduced graphene oxide (136.0 mA h $g^{-1}$ at 8 A $g^{-1}$) [43], $Ni_3S_2$@PANI core-shell nanosheets (242.8 mA h $g^{-1}$ at 5 A $g^{-1}$) [44], β-$Ni(OH)_2$/carbon nanofibers (150.0 mA h $g^{-1}$ at 50 mA $cm^{-2}$) [23], and α-β-$Ni_{1-x}Co_x(OH)_2$ (183.0 mA h $g^{-1}$ at 5 A $g^{-1}$) [45]. The specific capacities of the electrodes were calculated from the CD curves (Fig. S10), and the results were depicted in Fig. 4e. It could be clearly shown that the specific capacities of the Co-doped $NiMoO_4$ electrodes were much higher than that of pure $NiMoO_4$ electrode. Moreover, with the increase of cobalt doping, the specific capacity increased initially and then decreased rapidly, as shown in Fig. S11. The specific capacities were all maximal at the Co percentage of 15% at different current densities. Theoretically, the mechanism of charge storage could be estimated according to the equation: $i = av^b$, where $i$ is the peak current, $v$ is the scan rate, $a$ and $b$ are coefficients. The charge is stored dominantly determined by semi-infinite diffusion like batteries when $b$ is 0.5, while the value of 1 means a surface-controlled mechanism [13,44]. The $b$ values of anodic and cathodic peaks of CNMO-15 electrode were calculated to be 0.47 and 0.57, respectively (Fig. S12), revealing that the CNMO-15 electrode was a sort of battery-type material and the redox reaction was controlled dominantly by semi-infinite diffusion.

Moreover, the cycling tests were also conducted as shown in Fig. 4f. The CNMO-15 electrode maintained 95.7% of its initial specific capacity after 3000 cycles, while only 79.0% retention was kept by NMO electrode. The specific capacity of CNMO-15 increased gradually for the first 500 cycles mainly due to an activation process [46]. According to the SEM image of CNMO-15 electrode after

  

cycling tests (Fig. S13), the morphology of nanosheets kept almost unchanged, illustrating the superior structural stability. The overall promotion of electrochemical performance could also be demonstrated by the Nyquist plots inserted in Fig. 4f. The less internal resistance ($R_s$) of CNMO-15 (~2.7 Ω) relative to NMO (~5.3 Ω) indicated an enhanced electrical conductivity. Meanwhile, the smaller diameter of semicircle in the high-frequency region of CNMO-15 meant a strengthened charge transfer rate compared with NMO. And the slope in the low-frequency region of CNMO-15 was steeper than that of NMO, suggesting a faster ion diffusion rate [47]. Therefore, the CNMO-15 electrode exhibited the best electrochemical performance among these electrodes.

To evaluate the practical performance of CNMO-15, we have assembled an aqueous alkaline CNMO-15//Zn battery, where the CNMO-15 electrode served as the cathode and a commercial Zn plate as the anode with an aqueous electrolyte consisting of 1 mol $L^{-1}$ KOH and 0.01 mol $L^{-1}$ $Zn(CH_3COO)_2$. As depicted in Fig. 5a, the CV curves of the whole device displayed symmetric redox peaks at a wide range of operating voltage (1.4–2.0 V), testifying the highly reversibility of the redox reaction on the cathode. Simultaneously, the shape of CV curves at different scan rates kept almost unchanged, demonstrating the superior structural stability of the as-fabricated battery. The detailed charge storage mechanism of CNMO-15//Zn battery could be described as the following equations [21,22]:

Positive electrode:

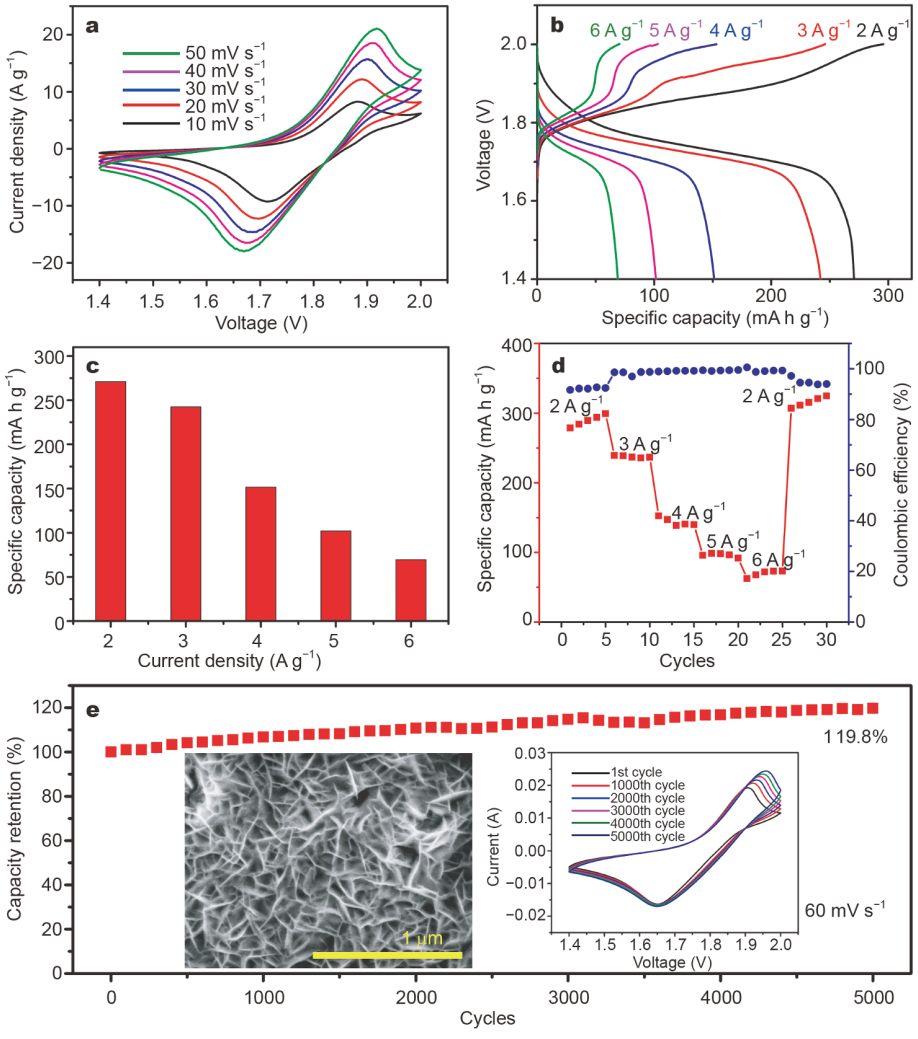


**Figure 5** (a) CV curves, (b) CD curves, (c) specific capacity, (d) rate performance and coulombic efficiency, and (e) cycling test of the CNMO-15//Zn battery. The insets of (e) are SEM image of the cathode after cycling test and CV curves of every 1000 cycles.

$$Ni^{2+} + 3OH^- \leftrightarrow NiOOH + H_2O + e^-; \quad (1)$$

Negative electrode:

$$[Zn(OH)_4]^{2-} + 2e^- \leftrightarrow Zn + 4OH^-; \quad (2)$$

Full cell reaction:

$$2Ni^{2+} + 2OH^- + [Zn(OH)_4]^{2-} \leftrightarrow 2NiOOH + Zn + 2H_2O. \quad (3)$$

Fig. 5b displays the CD curves of the CNMO-15//Zn battery under different current densities, exhibiting a satisfactory discharging voltage plateau of 1.70–1.75 V and high coulombic efficiency. As shown in Fig. 5c, the CNMO-15//Zn battery delivered a high specific capacity of 270.9 mA h $g^{-1}$ at 2 A $g^{-1}$, which was substantially higher than most of the reported Zn-ion batteries, such as NiO-carbon nanotube composite//Zn (155.0 mA h $g^{-1}$ at 1 A $g^{-1}$) [22], carbon cloth-carbon fiber@NiO//carbon cloth-carbon fiber@ZnO (203.0 mA h $g^{-1}$ at 0.5 mA $cm^{-2}$) [14], $NiS_2$/reduced graphene oxide//Zn (209.4 mA h $g^{-1}$ at 1 A $g^{-1}$) [43], $Ni_3S_2$/Ni nanosheets//Zn (148.0 mA h $g^{-1}$ at 0.2 A $g^{-1}$) [48], nickel nanowire arrays@Co-doped $Ni(OH)_2$//Zn (247.0 mA h $g^{-1}$ at 1 A $g^{-1}$) [24], and $NiCo_2O_4$ nanosheets/carbon cloth//Zn (183.1 mA h $g^{-1}$ at 1.6 A $g^{-1}$) [49]. Fig. 5d shows the rate performance and coulombic efficiency of CNMO-15//Zn battery. The coulombic efficiency was always over 90%, illustrating the fast charge transfer and rapid ion diffusion rates. Importantly, when cycling at current densities of 2, 3, 4, 5, and 6 A $g^{-1}$, the CNMO-15//Zn battery exhibited average capacities of 289.0, 230.1, 135.8, 96.1, and 69.6 mA h $g^{-1}$, respectively. And then an average discharge capacity of 315.8 mA h $g^{-1}$ could be recovered as the current density reduced to 2 A $g^{-1}$ after 25 cycles, demonstrating the outstanding rate and reversible stability. The assembled device delivered favorable energy efficiencies of 86.2%, 91.7%, 91.1%, 90.0% and 88.9% at current densities of 2, 3, 4, 5, and 6 A $g^{-1}$, respectively. Fig. 5e displays the cycling performance of the CNMO-15//Zn battery at a scan rate of 60 mV $s^{-1}$, and the specific capacity could hold 119.8% of its initial capacity after 5000 cycles. Such improved specific capacity could be chiefly attributed to the inflow of electrolyte into the enclosed space constructed by hierarchical nanosheets with pores, where more and more active sites inside started to participate in the redox reaction. Moreover, the constant contact in the electrode-electrolyte interfaces guaranteed the continuous reaction. Additionally, the nanosheet-like structure stayed nearly untouched after the cycling test according to the SEM image of CNMO-15 cathode (inset of Fig. 5e).

Energy density is a mainly obstacle constraining the practical application of Ni-Zn batteries. Fig. 6a compares the Ragone plots of the CNMO-15//Zn battery with other previously reported devices. Notably, the CNMO-15//Zn battery displayed a favorable energy density of 474.1 W h $kg^{-1}$ at 3.5 kW $kg^{-1}$, which still remained 118.8 W h $kg^{-1}$ at 10.3 kW $kg^{-1}$. The obtained properties were quite desirable, surpassing many other similar studies reported previously, such as nickel nanowire arrays@Co-doped $Ni(OH)_2$//Zn (148.5 W h $kg^{-1}$ at 1.7 kW $kg^{-1}$) [24], $Bi_2O_3/Bi_2Se_3$ nanoflowers//$NiCoSe_2$/$Ni_{0.85}Se$ nanoparticles (88.4 W h $kg^{-1}$ at 2.4 kW $kg^{-1}$) [50], NiO nanoflakes//α-$Fe_2O_3$ nanorods (15.6 W h $kg^{-1}$ at 7 kW $kg^{-1}$) [8], reduced $Co_3O_4$ nanosheets//Zn (295.5 W h $kg^{-1}$ at 0.8 kW $kg^{-1}$) [46], layered $Zn_2(OH)VO_4$//Zinc nanoflake array (65.0 W h $kg^{-1}$ at 6.2 kW $kg^{-1}$) [51], and $NiCo_2O_4$//3D hierarchical Bi (55.4 W h $kg^{-1}$ at 21.2 kW $kg^{-1}$) [12]. Particularly, the two as-fabricated CNMO-15//Zn batteries were connected in series to power six light emitting diodes (LED) indicators (1.5–2.0 V) for about 15 min after charging to 4.0 V

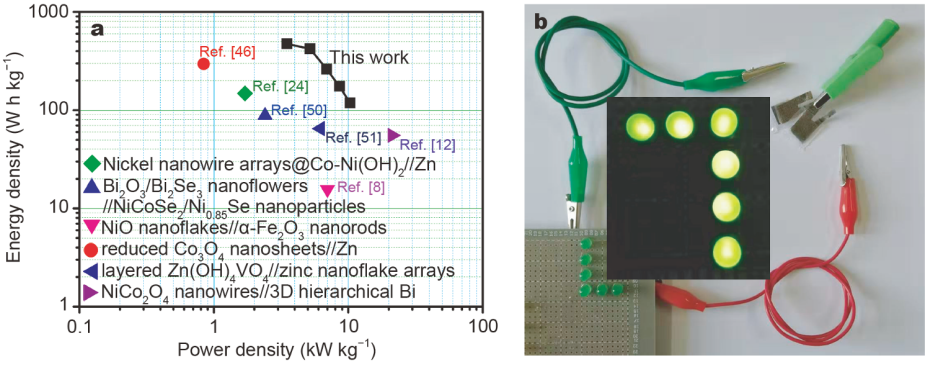


**Figure 6** (a) Ragone plot of the CNMO-15//Zn battery in comparison with previously reported devices. (b) Digital photo of the assembled device and lighted LEDs in darkness (inset).

(Fig. 6b). All these results illustrated that the doping of cobalt really did enhance the overall performance of $NiMoO_4$ and sequentially boosted the electrochemical properties of Ni-Zn batteries.

## CONCLUSIONS

In summary, the hierarchical Co-doped $NiMoO_4$ nanosheets have been successfully synthesized by an easy and accessible hydrothermal process followed by calcination treatment, and subsequently employed as the cathode for Ni-Zn battery. Mainly attributed to plentiful oxygen vacancies generated from the doping process, the electron transfer rate as well as the electrical conductivity gets improved, thus boosting the electrochemical performance. The obtained CNMO-15 electrode displays an enhanced specific capacity of 361.4 mA h $g^{-1}$ at 3 A $g^{-1}$ compared with NMO electrode (206.4 mA h $g^{-1}$ at 3 A $g^{-1}$), indicating the feasibility and high efficiency of cobalt doping. Furthermore, an aqueous rechargeable Ni-Zn battery with optimal electrochemical performance was assembled by CNMO-15 nanosheets as the cathode and a commercial zinc plate as the anode, which delivered a favorable energy density of 474.1 W h $kg^{-1}$ at 3.5 kW $kg^{-1}$ and powered six LEDs brightly for approximate 15 min, outperforming many other similar studies reported previously. In particular, there is no capacity decay with a 119.8% retention observed after 5000 cycles of the CNMO-15//Zn battery, illustrating the remarkable reversibility and cycling stability.

**Received 4 January 2020; accepted 8 March 2020; published online 8 April 2020**


1 Huang J, Wang Z, Hou M, *et al.* Polyaniline-intercalated manganese dioxide nanolayers as a high-performance cathode material for an aqueous zinc-ion battery. Nat Commun, 2018, 9: 2906
2 Pan H, Shao Y, Yan P, *et al.* Reversible aqueous zinc/manganese oxide energy storage from conversion reactions. Nat Energy, 2016, 1: 16039
3 Simon P, Gogotsi Y, Dunn B. Where do batteries end and supercapacitors begin? Science, 2014, 343: 1210–1211
4 Li YJ, Cui L, Da PF, *et al.* Multiscale structural engineering of Ni-doped CoO nanosheets for zinc-air batteries with high power density. Adv Mater, 2018, 30: 1804653
5 He J, Chen Y, Manthiram A. Metal sulfide-decorated carbon sponge as a highly efficient electrocatalyst and absorbant for polysulfide in high-loading $Li_2S$ batteries. Adv Energy Mater, 2019, 9: 1900584
6 Naveed A, Yang H, Shao Y, *et al.* A highly reversible Zn anode with intrinsically safe organic electrolyte for long-cycle-life batteries. Adv Mater, 2019, 31: 1900668
7 Li X, Guan C, Hu Y, *et al.* Nanoflakes of Ni–Co LDH and $Bi_2O_3$ assembled in 3D carbon fiber network for high-performance aqueous rechargeable Ni/Bi battery. ACS Appl Mater Interfaces, 2017, 9: 26008–26015
8 Sarkar D, Shukla A, Sarma DD. Substrate integrated nickel–iron ultrabattery with extraordinarily enhanced performances. ACS Energy Lett, 2016, 1: 82–88
9 Lei D, Lee DC, Magasinski A, *et al.* Performance enhancement and side reactions in rechargeable nickel–iron batteries with nanostructured electrodes. ACS Appl Mater Interfaces, 2016, 8: 2088–2096
10 Zhao X, Ma L, Shen X. Co-based anode materials for alkaline rechargeable Ni/Co batteries: a review. J Mater Chem, 2012, 22: 277–285
11 Gao XP, Yao SM, Yan TY, *et al.* Alkaline rechargeable Ni/Co batteries: cobalt hydroxides as negative electrode materials. Energy Environ Sci, 2009, 2: 502–505
12 Zeng Y, Lin Z, Meng Y, *et al.* Flexible ultrafast aqueous rechargeable Ni//Bi battery based on highly durable single-crystalline bismuth nanostructured anode. Adv Mater, 2016, 28: 9188–9195
13 Hao Z, Xu L, Liu Q, *et al.* On-chip Ni-Zn microbattery based on hierarchical ordered porous $Ni@Ni(OH)_2$ microelectrode with ultrafast ion and electron transport kinetics. Adv Funct Mater, 2019, 29: 1808470
14 Liu J, Guan C, Zhou C, *et al.* A flexible quasi-solid-state nickel-zinc battery with high energy and power densities based on 3D electrode design. Adv Mater, 2016, 28: 8732–8739
15 Meng L, Lin D, Wang J, *et al.* Electrochemically activated nickel–carbon composite as ultrastable cathodes for rechargeable nickel–zinc batteries. ACS Appl Mater Interfaces, 2019, 11: 14854–14861
16 Huang M, Li M, Niu C, *et al.* Recent advances in rational electrode designs for high-performance alkaline rechargeable batteries. Adv Funct Mater, 2019, 29: 1807847
17 Wang R, Han Y, Wang Z, *et al.* Nickel@nickel oxide core-shell electrode with significantly boosted reactivity for ultrahigh-energy and stable aqueous Ni-Zn battery. Adv Funct Mater, 2018, 28: 1802157
18 Lee DU, Fu J, Park MG, *et al.* Self-assembled $NiO/Ni(OH)_2$ nanoflakes as active material for high-power and high-energy hybrid rechargeable battery. Nano Lett, 2016, 16: 1794–1802
19 Shang W, Yu W, Tan P, *et al.* Achieving high energy density and efficiency through integration: progress in hybrid zinc batteries. J Mater Chem A, 2019, 7: 15564–15574
20 Tan P, Chen B, Xu H, *et al.* Nanoporous $NiO/Ni(OH)_2$ plates incorporated with carbon nanotubes as active materials of rechargeable hybrid zinc batteries for improved energy efficiency and high-rate capability. J Electrochem Soc, 2018, 165: A2119–A2126
21 Zeng Y, Lai Z, Han Y, *et al.* Oxygen-vacancy and surface modulation of ultrathin nickel cobaltite nanosheets as a high-energy cathode for advanced Zn-ion batteries. Adv Mater, 2018, 30: 1802396
22 Wang X, Li M, Wang Y, *et al.* A Zn–NiO rechargeable battery with long lifespan and high energy density. J Mater Chem A, 2015, 3: 8280–8283
23 Jian Y, Wang D, Huang M, *et al.* Facile synthesis of $Ni(OH)_2$/carbon nanofiber composites for improving NiZn battery cycling life. ACS Sustain Chem Eng, 2017, 5: 6827–6834
24 Xu C, Liao J, Yang C, *et al.* An ultrafast, high capacity and superior longevity Ni/Zn battery constructed on nickel nanowire array film. Nano Energy, 2016, 30: 900–908
25 Gong M, Li Y, Zhang H, *et al.* Ultrafast high-capacity NiZn battery with NiAlCo-layered double hydroxide. Energy Environ Sci, 2014, 7: 2025–2032


  

26 Chen C, Yan D, Luo X, *et al.* Construction of core–shell Ni-$MoO_4$@Ni-Co-S nanorods as advanced electrodes for high-performance asymmetric supercapacitors. ACS Appl Mater Interfaces, 2018, 20: 4662–4671
27 Qing C, Yang C, Chen M, *et al.* Design of oxygen-deficient $NiMoO_4$ nanoflake and nanorod arrays with enhanced supercapacitive performance. Chem Eng J, 2018, 354: 182–190
28 Liu Z, Zhan C, Peng L, *et al.* A $CoMoO_4$–$Co_2Mo_3O_8$ heterostructure with valence-rich molybdenum for a high-performance hydrogen evolution reaction in alkaline solution. J Mater Chem A, 2019, 7: 16761–16769
29 Zhang Z, Zhang H, Zhang X, *et al.* Facile synthesis of hierarchical $CoMoO_4$@$NiMoO_4$ core–shell nanosheet arrays on nickel foam as an advanced electrode for asymmetric supercapacitors. J Mater Chem A, 2016, 4: 18578–18584
30 Cheng D, Yang Y, Xie J, *et al.* Hierarchical $NiCo_2O_4$@$NiMoO_4$ core–shell hybrid nanowire/nanosheet arrays for high-performance pseudocapacitors. J Mater Chem A, 2015, 3: 14348–14357
31 Zhang P, Zhou J, Chen W, *et al.* Constructing highly-efficient electron transport channels in the 3D electrode materials for high-rate supercapacitors: the case of $NiCo_2O_4$@$NiMoO_4$ hierarchical nanostructures. Chem Eng J, 2017, 307: 687–695
32 Yang J, Liu W, Niu H, *et al.* Ultrahigh energy density battery-type asymmetric supercapacitors: $NiMoO_4$ nanorod-decorated graphene and graphene/$Fe_2O_3$ quantum dots. Nano Res, 2018, 11: 4744–4758
33 Sharma GP, Pala RGS, Sivakumar S. Ultrasmall $NiMoO_4$ robust nanoclusters-active carbon composite for high performance extrinsic pseudocapacitor. Electrochim Acta, 2019, 318: 607–616
34 Lei X, Ge S, Tan Y, *et al.* Bimetallic phosphosulfide Zn–Ni–P–S nanosheets as binder-free electrodes for aqueous asymmetric supercapacitors with impressive performance. J Mater Chem A, 2019, 7: 24908–24918
35 Huang J, Wei J, Xiao Y, *et al.* When Al-doped cobalt sulfide nanosheets meet nickel nanotube arrays: a highly efficient and stable cathode for asymmetric supercapacitors. ACS Nano, 2018, 12: 3030–3041
36 Ling T, Zhang T, Ge B, *et al.* Well-dispersed nickel- and zinc-tailored electronic structure of a transition metal oxide for highly active alkaline hydrogen evolution reaction. Adv Mater, 2019, 31: 1807771
37 Wang R, Lu Y, Zhou L, *et al.* Oxygen-deficient tungsten oxide nanorods with high crystallinity: promising stable anode for asymmetric supercapacitors. Electrochim Acta, 2018, 283: 639–645
38 Chiu KL, Lin LY. Applied potential-dependent performance of the nickel cobalt oxysulfide nanotube/nickel molybdenum oxide nanosheet core–shell structure in energy storage and oxygen evolution. J Mater Chem A, 2019, 7: 4626–4639
39 Lin J, Yao L, Li Z, *et al.* Hybrid hollow spheres of carbon@$Co_xNi_{1-x}MoO_4$ as advanced electrodes for high-performance asymmetric supercapacitors. Nanoscale, 2019, 11: 3281–3291
40 Xu K, Ma S, Shen Y, *et al.* $CuCo_2O_4$ nanowire arrays wrapped in metal oxide nanosheets as hierarchical multicomponent electrodes for supercapacitors. Chem Eng J, 2019, 369: 363–369
41 Ruan Y, Lv L, Li Z, *et al.* Ni nanoparticles@Ni–Mo nitride nanorod arrays: a novel 3D-network hierarchical structure for high areal capacitance hybrid supercapacitors. Nanoscale, 2017, 9: 18032–18041
42 Lu Z, Wu X, Lei X, *et al.* Hierarchical nanoarray materials for advanced nickel–zinc batteries. Inorg Chem Front, 2015, 2: 184–187
43 Shi W, Mao J, Xu X, *et al.* An ultra-dense $NiS_2$/reduced graphene oxide composite cathode for high-volumetric/gravimetric energy density nickel–zinc batteries. J Mater Chem A, 2019, 7: 15654–15661
44 Zhou L, Zhang X, Zheng D, *et al.* $Ni_3S_2$@PANI core–shell nanosheets as a durable and high-energy binder-free cathode for aqueous rechargeable nickel–zinc batteries. J Mater Chem A, 2019, 7: 10629–10635
45 Huang M, Xu Z, Hou C, *et al.* Intermediate phase α-β-$Ni_{1-x}Co_x$-$(OH)_2$/carbon nanofiber hybrid material for high-performance nickel-zinc battery. Electrochim Acta, 2019, 298: 127–133
46 Lu Y, Wang J, Zeng S, *et al.* An ultrathin defect-rich $Co_3O_4$ nanosheet cathode for high-energy and durable aqueous zinc ion batteries. J Mater Chem A, 2019, 7: 21678–21683
47 Zhang H, Liu Q, Wang J, *et al.* Boosting the Zn-ion storage capability of birnessite manganese oxide nanoflorets by $La^{3+}$ intercalation. J Mater Chem A, 2019, 7: 22079–22083
48 Hu P, Wang T, Zhao J, *et al.* Ultrafast alkaline Ni/Zn battery based on Ni-foam-supported $Ni_3S_2$ nanosheets. ACS Appl Mater Interfaces, 2015, 7: 26396–26399
49 Zhang H, Zhang X, Li H, *et al.* Flexible rechargeable Ni//Zn battery based on self-supported $NiCo_2O_4$ nanosheets with high power density and good cycling stability. Green Energy Environ, 2018, 3: 56–62
50 Meng A, Yuan X, Shen T, *et al.* One-step synthesis of flower-like $Bi_2O_3$/$Bi_2Se_3$ nanoarchitectures and $NiCoSe_2$/$Ni_{0.85}Se$ nanoparticles with appealing rate capability for the construction of high-energy and long-cycle-life asymmetric aqueous batteries. J Mater Chem A, 2019, 7: 17613–17625
51 Chao D, Zhu CR, Song M, *et al.* A high-rate and stable quasi-solid-state zinc-ion battery with novel 2D layered zinc orthovanadate array. Adv Mater, 2018, 30: 1803181


**Acknowledgements** This work was financially supported by the National Natural Science Foundation of China (51602049), the Fundamental Research Funds for the Central Universities (2232017D-15, GSIF-DH-M-2020002), and China Postdoctoral Science Foundation (2017M610217 and 2018T110322).

**Author contributions** Shen Y and Zhang K performed the experiments and wrote the article. Liu Q, Li Z and Cui Z conducted the characterization and data analysis. Yang F, Zou R, Hu J and Xu K proposed the experimental design. All authors contributed to the general discussion.

**Conflict of interest** The authors declare no conflict of interest.

**Supplementary information** Supporting data are available in the online version of the paper.

  

**Yuenian Shen** is currently a postgraduate student in the College of Materials Science and Engineering, Donghua University. His current interest focuses on the transition metal oxides for electrochemical energy storage and conversion applications.

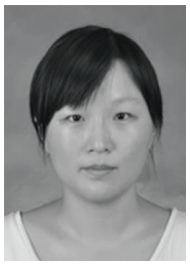

**Qian Liu** is currently working at Donghua University. She received her BS degree in physics from Ludong University (2010) and her PhD in material science from Donghua University (2015). Her current research interests are focusing on 1D and 2D nanomaterials' manipulation, transformations and atomic level understanding of electromechanical, energy conversion and energy storage systems.

**Kaibing Xu** received his PhD degree from Donghua University in 2015. Currently, he works in the Research Center for Analysis and Measurement at Donghua University. His research focuses on rational design and synthesis of nanocomposite materials for applications in electrochemical energy storage and conversion such as supercapacitors, alkaline rechargeable batteries and lithium ion batteries.

## 富氧空位的钴掺杂$NiMoO_4$纳米片用于高能量密度和循环稳定性的水系镍锌电池

沈越年[1], 张可[4], 杨方[4], 李志豪[1], 崔哲[1], 邹儒佳[1], 刘倩[3*], 胡俊青[5], 徐开兵[1,2*]

**摘要** 提高能量密度和循环稳定性对推广水系可充电镍锌电池的广泛应用至关重要. 我们采用一种简易的合成方法构建了Co掺杂$NiMoO_4$纳米片, 并将其作为正极材料用于高性能镍锌电池. 得益于导电性和氧空位浓度的大幅度提升, 钴掺杂量为15%的电极材料(CNMO-15)表现出突出的比容量及循环稳定性, 在3 A $g^{-1}$的电流密度下其容量高达361.4 mA h $g^{-1}$. 此外, 以CNMO-15为正极组装的镍锌电池(CNMO-15//Zn)也展现了优异的比容量(在2 A $g^{-1}$的电流密度下高达270.9 mA h $g^{-1}$), 以及高能量密度(在3.5 kW $kg^{-1}$的功率密度下高达474.1 W h $kg^{-1}$)和功率密度(在118.8 W h $kg^{-1}$的能量密度下高达10.3 kW $kg^{-1}$). 值得注意的是, 该电池在循环5000圈后容量没有损失, 保留了初始容量的119.8%, 表现出优异的循环稳定性. 本研究可以为未来构建高能量密度和优异循环稳定性的镍锌电池提供非常有价值的参考.

  